Higher-order nodal hinge states in doped superconducting topological insulator

Sayed Ali Akbar Ghorashi,[1,*] Jennifer Cano,[1,2] Enrico Rossi,[3] and Taylor L. Hughes[4]
[1]*Department of Physics and Astronomy, Stony Brook University, Stony Brook, New York 11794, USA*
[2]*Center for Computational Quantum Physics, Flatiron Institute, New York, New York 10010, USA*
[3]*Department of Physics, William & Mary, Williamsburg, Virginia 23187, USA*
[4]*Department of Physics and Institute for Condensed Matter Theory, University of Illinois at Urbana-Champaign, Illinois 61801, USA*

(Received 7 December 2022; accepted 25 August 2023; published 7 September 2023)

Doped strong topological insulators are one of the most promising candidates to realize a fully gapped three-dimensional topological superconductor (TSC). In this Letter, we revisit this system and reveal a possibility for higher-order topology which was previously missed. We find that over a finite range of doping, the Fu-Berg superconducting pairing can give rise to both Majorana surface states and nodal hinge states. Interestingly, we observe the coexistence of surface and hinge modes in the superconducting state only when there are both bulk and surface Fermi surfaces in the normal state. Also, we find that the hinge modes can appear for normal states consisting of doped strong or weak topological insulators. In summary, this work may allow for the discovery of superconducting hinge modes in a well explored class of materials, i.e., doped strong or weak topological insulators.

DOI: 10.1103/PhysRevB.108.094504

Introduction. Since its discovery, the notion of topological phases has been extended to almost all aspects of condensed matter physics and related fields, such as photonics and cold-atomic gases. The initial topological AZ classification table has been extended multiple times and now includes crystalline phases and even gapless phases [1–3]. One of the most recent additions are the so-called nth-order topological phases which possess gapless states on boundaries having codimension $d_c = n$ [4–16]. Hybrid-order topological phases where first and second order boundary states coexist have also been discovered [14,17,18]. Despite the many experimentally verifiable material candidates for topological insulators and topological semimetals, the search for topological superconductors (TSC) has proven to be more challenging. The challenge lies in finding a single material in which the band structure and interaction-driven superconductivity conspire to form a topological phase. Finding a higher-order generalization of TSCs usually requires additional bandstructure features and/or exotic pairing, further complicating the search for experimental candidates [19].

In this Letter, we revisit a family of promising solid state candidates for first order 3D TSCs: doped 3D topological insulators with time-reversal symmetry [20–25]. We show that, remarkably, a system exhibiting the Fu-Berg interorbital singlet pairing [21] can be tuned into a hybrid-order TSC (HyTSC) phase with coexisting surface and hinge states by doping such that both bulk and surface Fermi surfaces are present in the normal state. The surface Majorana cones are protected by time-reversal symmetry, while the hinge modes are protected by mirror symmetries, so they can be manipulated independently. Furthermore, we find that the HyTSC state can be achieved from a strong or weak TI normal state. We demonstrate these phenomena using a conventional TI model with cubic symmetry. We then briefly show that the hinge states persist even in the absence of cubic symmetry (e.g., in the presence of hexagonal warping) [26], which might be relevant to realistic experimental contexts. Our main results are summarized in Fig. 1.

Model. We start from a model of a superconducting TI with the BdG Hamiltonian $H(\mathbf{k}) = \sum \Psi^\dagger h(k) \Psi$ [21], where

$$h(\mathbf{k}) = \begin{bmatrix} H_{TI}(\mathbf{k}) - \mu & -i\Delta \\ i\Delta^\dagger & -H_{TI}^T(-\mathbf{k}) + \mu \end{bmatrix}. \tag{1}$$

and

$$H_{TI}(\mathbf{k}) = \left(M + t_0 \sum_i \cos(k_i) \right) \kappa_z \sigma_0 + t_1 \sum_i \sin(k_i) \kappa_x \sigma_i, \tag{2}$$

where κ_a, σ_b $a, b = x, y, z$ are Pauli matrices in orbital and spin space, respectively, and κ_0, σ_0 are identity matrices. In the following we set $t_0 = t_1 = 1$. For the ranges $1 < |M| < 3$, $0 < |M| < 1$, and $|M| > 3$, H_{TI} represents a time-reversal invariant insulator with strong, weak, and trivial topology, respectively. The pairing term is chosen to be the Fu-Berg pairing [21]: $\Delta = \delta_0 \kappa^1 \sigma^2$, where δ_0 is the pairing amplitude. It has been shown that this interorbital, odd-parity pairing Δ is a relevant pairing instability in superconducting doped TIs [21]. The Hamiltonian (1) preserves both time-reversal and inversion symmetries, as well as fourfold rotation, C_4^z. In the following we will discuss the HyTSC phase in this system, which exhibits coexisting Majorana surface states and mirror-protected nodal hinge states.

*sayedaliakbar.ghorashi@stonybrook.edu

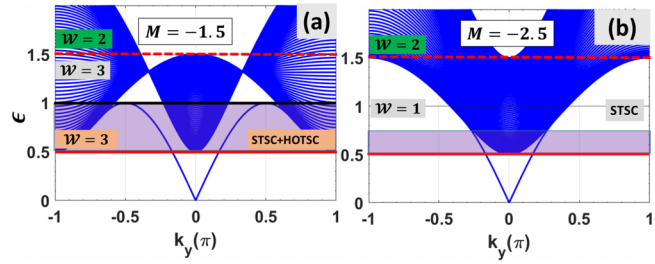

FIG. 1. Summary of results. (a) For TIs described by H_{TI} with $|M| < 2$, there are three distinct topological superconducting phases achievable by doping if we assume the bulk pairing takes the Fu-Berg pairing [21]. As an example, for $M = -1.5$, when increasing μ from zero the system evolves to a strong TSC (STSC) (red solid line) with a winding number $\mathcal{W} = 3$. By further increasing μ into the region where bulk and surface Fermi-surfaces coexist in the normal state (shaded purple region), we find a STSC that coexists with a HOTSC with nodal hinge states (labelled by STSC + HOTSC). Upon further increasing μ, the hinge states vanish (black solid line), realizing a STSC. Finally, another TSC appears having $\mathcal{W} = 2$ (red dashed line) as μ increases further. In contrast, for (b) $|M| > 2$ we find STSC phases but we do not find a HOTSC phase and corresponding hinge states.

Normal phase. While the precise value of $|M|$ in each of the ranges listed above has no bearing on the topological properties of the insulating state, it can, however, have a notable effect on the nature of the Fermi surfaces at a given Fermi level. The different Fermi surface structures are correlated with the resulting TSC phases. For illustration we show representative examples of the normal phase spectrum of H_{TI} for values of $M = -2.5,\ -1.5,\ -0.5$ in Figs. 2(a1)–2(c1). These spectra are calculated for open boundaries in z, but periodic in x, y. We show a particular $k_x = 0$ slice where one can see the bulk gap (which is the same size for all three values of M) and midgap surface states. The values $M = -2.5, -1.5$ are strong TIs, while $M = -0.5$ is a weak TI which has an even number of surface Dirac cones (only one is visible at $k_x = 0$ because the other is centered around $k_x = \pi$).

The first two values of M, despite being in the same topological phase, have qualitative differences in their surface and bulk Fermi surfaces that turn out to be important for the characterization of the TSC phase. To illustrate this, let us focus on the red bars marked in Figs. 2(a1)–2(c1). These denote a window of energy in which the surface and bulk states coexist (which we denote the surf-bulk region), and which varies as M changes. The coexistence region is generic as there are only two fine-tuned values of $M = 0, -2$ [see Fig. 4(a1)] where the system is insulating and the surf-bulk region vanishes. We also note that the closer the value of M is to the weak-to-strong TI phase transition at $M = -1$, the wider the surf-bulk region becomes. We find that as long as there is a finite surf-bulk region, the weak or strong topological nature of the normal phase does not have a major effect on the appearance of hinge modes, as we discuss below. This and the fact the phenomena we examine survive to the weak pairing limit are an indication that the physics is driven by the Fermi surfaces and not the topology of the occupied bands. We also note that the evolution of the surface Fermi surfaces as one raises the chemical potential can be different within the same topological phase, e.g., $M = -2.5, -1.5$, in Figs. 2(a1) and 2(b1). In the case of $M = -2.5$ the surface Dirac cone at the Γ point evolves into bulk Fermi surfaces encircling the Γ point, while for $M = -1.5$, the surface Dirac point evolves to bulk Fermi surfaces centered at $(k_x, k_y) = (0, \pi)$ and $(\pi, 0)$.

Superconducting phase. Now let us consider the BdG quasiparticle spectrum for this system. The bulk (first order) topology protected by time-reversal symmetry can be characterized using the 3D winding number [25,27]:

$$\mathcal{W} = \frac{1}{48\pi^2}\int d\mathbf{k}\epsilon_{ijk}[\mathcal{S}(h^{-1}\partial_i h)(h^{-1}\partial_j h)(h^{-1}\partial_k h)], \quad (3)$$

where $\mathcal{S}$ is a chiral symmetry that acts as $\mathcal{S}h(\mathbf{k})\mathcal{S}^{-1} = -h(\mathbf{k})$. For the DIII class, $\mathcal{W}$ takes integer values and guarantees the existence of the surface Majorana cones when it is nonvanishing [25,27,28]. In our model, at a representative value of $\delta_0 = 0.4$, for example, the bulk superconducting spectrum undergoes topological phase transitions as a function of μ.

In Fig. 1, we show $\mathcal{W}$ over a range of μ for two representative values of $M = -2.5, -1.5$ (see [29] for more detail). Both values of M have a topological phase transition at $\mu_{c1} = E_g - \delta_0/2 = 0.3$, where E_g is the insulating gap. For $|M| < 2$ the winding number transitions from zero to $\mathcal{W} = 3$ at μ_{c1} while for $|M| > 2$ it transitions to $\mathcal{W} = 1$. In the ultra weak pairing limit as $\delta_0 \to 0$ this difference can be ascribed to the number of (spin-degenerate) Fermi surfaces affected by the pairing, i.e., for $|M| < 2$ there are three closed Fermi surfaces and each one surrounds one of the X, Y, and Z points in the BZ, while for $|M| > 2$ there is a single closed Fermi surface surrounding the Γ point. The conventional bulk-boundary correspondence indicates that a higher-winding number signals higher numbers of stable surface states. Therefore, even at the level of first-order topology the doped $|M| < 2$ and $|M| > 2$ insulators generate different superconducting topological phases, even though their corresponding normal phases are topologically equivalent [30]. Now, let us examine the surface states in the superconducting phases more closely. In Figs. 2(a2)–2(c2) we show the surface corresponding to the Hamiltonian Eq. (1) with open boundaries in the z direction, for $M = -2.5,\ -1.5,\ -0.5$ at fixed values of $\delta_0 = 0.4$, $\mu = 0.6$; the other surfaces behave similarly due to the crystal symmetries. Note that the chemical potential is within the surf-bulk region denoted by the red bars in Figs. 2(a1)–2(c1). For $M = -2.5$, there is only one Majorana cone located at $k_x = k_y = 0$ in the reduced BZ, while the phase with $M = -1.5$ hosts three Majorana cones: one at $k_x = k_y = 0$ and two others at $(k_x, k_y) = (0, \pi), (\pi, 0)$, in agreement with the associated bulk invariants of $\mathcal{W} = 1$ and 3, respectively. In the $\mathcal{W} = 3$ phase there are two gapless points on the $k_x = 0$ and $k_y = 0$ lines; along these lines, the surface states attach to each other and are free floating, i.e., they are detached from the bulk states. This surface-state connectivity requires $|\mathcal{W}| > 1$.

Remarkably, when cutting the surface again to form hinges the phase with $\mathcal{W} = 3$ has nodal hinge states when the chemical potential is in the surf-bulk region. To see this explicitly, in Fig. 3 we have plotted the evolution of the superconducting surface and hinge states versus μ for a TI with $M = -1.5$. We find that the hinge states appear only when $0.5 < \mu < 1$, which corresponds to the surf-bulk region in the normal phase,

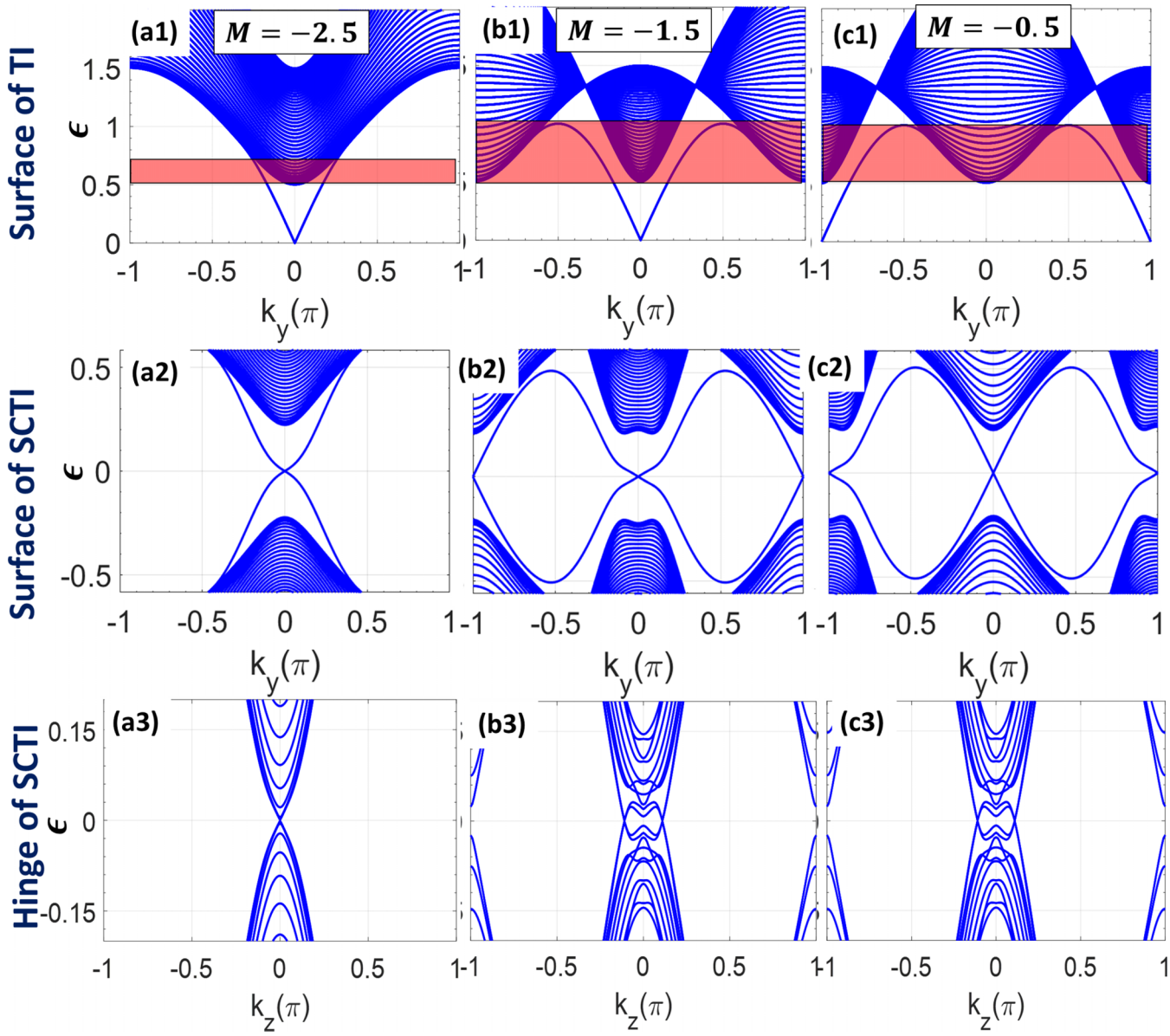

FIG. 2. Emergence of hinge states for $|M| < 2$. (a1)–(c1) Spectrum with open boundaries in the z direction (at $k_x = 0$) of insulating phases of H_{TI} in Eq. (2) with $M = -2.5$ (strong TI),-1.5 (strong TI),-0.5 (weak TI), respectively. (a2)–(c2) and (a3)–(c3) show surface (open in z direction) and hinge (open in x and y directions) spectra of superconducting phases corresponding to (a1)–(c1), respectively. The shaded region denotes the range of chemical potentials for which bulk and surface Fermi surfaces coexist in the normal state. The parameters $\delta_0 = 0.4$, $\mu = 0.6$ (in shaded area) are used for all superconducting spectra.

[c.f., Fig. 2(b1)], but not the full span of the $\mathcal{W} = 3$ phase. We also note that, despite having its own surf-bulk coexistence region, the $\mathcal{W} = 1$ phase does not exhibit such hinge states.

We can understand more about the nature and protection of the hinge states by considering the low-energy Hamiltonian on a single hinge. Consider the critical point of the hinge states at $M = -1.5$, $\delta_0 = 0.4$, and $\mu = 1.0$ as shown in Fig. 3(d2). At this critical point the energy spectrum of the modes on a single hinge consists of two parabolas that touch at the high symmetry point $k_z = 0$. The critical Hamiltonian on a single hinge is hence given by

$$H_{\text{hinge}}(k_z) = k_z^2 \sigma^z. \tag{4}$$

This low-energy Hamiltonian has a particle-hole symmetry implemented by $C = \sigma^x$, such that $CH_{\text{hinge}}(k_x)C^{-1} = -H^T_{\text{hinge}}(-k_z)$. We also want the Hamiltonian to have mirror symmetry M_z, and there are two choices: $M_z = \mathbb{I}$ or $M_z = \sigma^z$. Both choices lead to $M_z H_{1D}(k_z) M_z^{-1} = H_{1D}(-k_z)$. However, the bulk Hamiltonian has operators that satisfy $[C, M_z] = 0$ so we choose $M_z = \mathbb{I}$ (also, if we chose $M_z = \sigma^z$ the mirror symmetric spectrum would not match the numerical results) [31].

The generic Hamiltonian of the hinge states satisfying C and M_z is given by

$$H^{\mathbb{I}}_{1D}(k_z) = k_z^2 \sigma^z + (\mu - 1)\sigma^z, \tag{5}$$

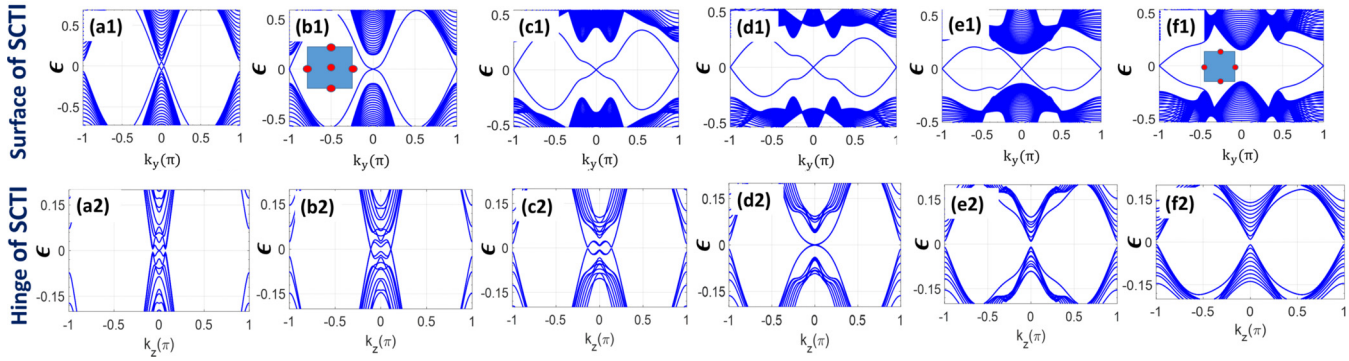

FIG. 3. The evolution of surface (a1)–(f1) and hinge (a2)–(f2) states in the superconducting strong TI versus chemical potential μ. The values of $\mu = 0.4, 0.6, 0.8, 1, 1.3, 1.6$ are used for (a)–(f), respectively. Insets in (b1) and (f1) show the 2D arrangement of surface nodes in BZ. The parameters $M = -1.5$, $\delta_0 = 0.4$ are used throughout.

to second order in k_z. This Hamiltonian has energy bands $E(k_z) = \pm(k_z^2 + \mu - 1)$. If $\mu > 1$, the two parabolas lift off each other and generate a gapped phase as seen in numerics. If $\mu < 1$, the base of the upper parabola moves below the peak of the lower parabola leaving gapless, linear crossing points at $k_z^* = \pm\sqrt{|\mu - 1|}$.

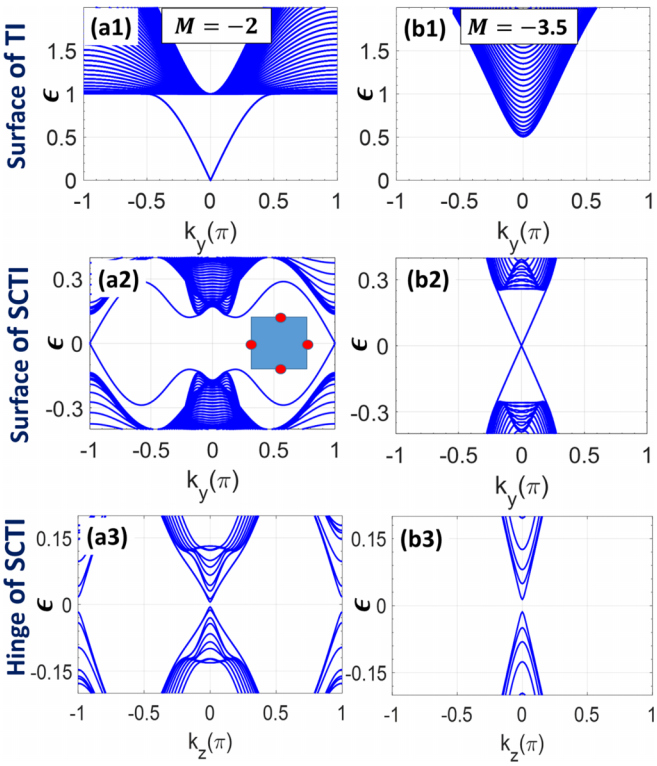

FIG. 4. Absence of hinge states for $M = -2, -3.5$ when coexisting surface and bulk states are absent. Surface states of the normal phase, and surface and hinge states of the superconducting phase, for $M = -2$ (a1)–(a3) and $M = -3.5$ (b1)–(b3), respectively. The parameters $\delta_0 = 0.4$; $\mu = 1.2$(a2), (a3); and $\delta_0 = 0.4$, $\mu = 0.8$ (b2), (b3) are used. Insets in (a2) show the 2D arrangement of surface nodes in BZ.

We expand the Hamiltonian around the two k_z^* to find the four-band Hamiltonian for the two valleys:

$$H_V(k_z) = 2\sqrt{|\mu - 1|}k_z\tau^z\sigma^z, \tag{6}$$

where τ^z acts in the valley space and k_z represents the deviation away from $\pm k_z^*$ in each block, respectively. Both mirror and particle hole exchange the valleys since they flip the sign of the k_z momentum. Hence, we would expect that in the valley Hamiltonian $C^V = \tau^x\sigma^x$ and $M_z^V = \tau^x\mathbb{I}$. One can check that our Hamiltonian in the valley representation still has both C and M_z symmetry and that $[C^V, M_z^V] = 0$ still holds.

To check the stability of the gapless hinge modes we enumerate all possible gapping terms. The full list is $(1)\tau^z\sigma^x$, $(2)\tau^z\sigma^y$, $(3)\mathbb{I}\sigma^x$, $(4)\mathbb{I}\sigma^y$, $(5)\tau^x\sigma^z$, $(6)\tau^x\mathbb{I}$, $(7)\tau^y\sigma^z$, $(8)\tau^y\mathbb{I}$. Each mass term breaks a symmetry, specifically: mass (1) and (2) break mirror, mass (3) and (4) break particle hole, mass (5) breaks translation, mass (6) breaks translation and particle hole, mass (7) breaks translation and mirror, and mass (8) breaks particlehole, mirror, and translation. Let us ignore translation for a moment. We find that if we do not have mirror we can add for example mass (1). If we do not have particle hole we can add mass (3) so they are both required for protection. If we have both symmetries then all masses except (5) are forbidden, and we can forbid (5) by assuming translation symmetry along the hinge, as is implicitly required to protect nodal points in general. While one might worry that doping breaks the crystalline symmetries, doped topological superconductors show robust signatures of translation symmetry in ARPES [32], and doped topological crystalline insulators have shown robust signatures of symmetry-protected hinge states [33].

Now let us consider the classification of the nodal points. Suppose we make two identical copies of our Hamiltonian

$$H_V^{\text{double}}(k_z) = 2\sqrt{|\mu - 1|}k_z\mathbb{I}\tau^z\sigma^z. \tag{7}$$

Because the copies are identical, the symmetries are $C^V = \mathbb{I}\tau^x\sigma^x$ and $M_z^V = \mathbb{I}\tau^x\mathbb{I}$. Now consider mass (3) which broke only particle-hole symmetry. For the doubled Hamiltonian we can have the mass $(3')\mu^y\mathbb{I}\sigma^x$, where μ^a are Pauli matrices in the double copy space. Since we have added an imaginary matrix as compared to mass (3), this mass term will now preserve particle hole. Adding the extra μ^y factor does not

affect translation or mirror so this mass term now obeys all of the symmetries. Hence, the stability classification of the nodal points is $\mathbb{Z}_2$ since two identical copies can be gapped while preserving all of the symmetries. Thus, while one hinge is stable in the presence of the symmetries mentioned, if two hinges are coupled then the modes can be gapped out.

It is important to note that the surface and hinge states can be independently gapped out; therefore, time-reversal symmetry does not play any role in the protection of hinge states (see Table I in [29] for details).

We now comment on two specific cases which are particularly instructive. Figure 4 shows the surface (normal and superconducting) and hinge (superconducting) plots for $M = -2$ and $M = -3.5$. The former is a strong TI, while the latter is a trivial insulator, and both cases lack a surf-bulk region. We make two remarks: (i) while the emergence of first-order topological superconductivity does not require nontrivial bulk topology of the normal phase, we find hinge states in this system only when the normal phase possesses surface states generated by either weak or strong topology; and (ii) if we pick a value of $|M| \sim 2$ and fix μ such that hinge states are generated, then tuning through $|M| = 2$ while keeping μ fixed will drive a transition between the HyTSC phase and a first-order topological superconductor since the normal state for $|M| = 2$ does not exhibit coexisting surface and bulk Fermi surfaces for any value of μ.

Discussion. We now make a few final remarks. First, as we have shown, the higher-order gapless hinge states appear for both weak and strong TIs. Hence, our finding facilitates the experimental realization of hinge states by broadening the range of possible material candidates. Second, in many realistic TI materials, such as Bi_2Te_3, the surface states are subject to hexagonal warping [26]. In the Supplemental Material [29] we investigate the effect of a particular type of hexagonal warping and find that hinge states can still appear, though the deformation caused by the warping affects the parameter ranges and spatial location of the hinge states compared to the case with C_4^z symmetry studied here. A more detailed analysis of the effects of hexagonal warping is left for future work. As a last remark, we note that recently, there have been many developments in characterization of TSCs via symmetry indicators [34–37]. A particular example is a recent work [18], which proposed a 3D hybrid-order TSC in presence of C_4^z symmetry using a more complex tight-binding model and pairing. However, the invariants introduced there cannot be applied to our system as the hinge states we find are more akin to a 1D nodal superconductor protected by mirror symmetry, and do not appear at high-symmetry momenta.

Finally, we emphasize that the physics discussed in this work opens up a new avenue toward the experimental discovery of HOTSCs using well-studied material candidates, in either weak or strong TIs phases, and calls for further careful experimental studies in these systems, especially in scenarios where the chemical potential intersects both bulk states and topological surface states.

Acknowledgments. We thank Masatoshi Sato for useful discussion. S.A.A.G. acknowledges support from the Air Force Office of Scientific Research (Grant No. FA9550-20-1-0260). E.R. acknowledges support from DOE-BES, Grant No. DE-SC0022245. T.L.H. thanks ARO MURI W911NF2020166 for support. J.C. is partially supported by the Alfred P. Sloan Foundation through a Sloan Research Fellowship and acknowledges the support of the Flatiron Institute, a division of the Simons Foundation.

[1] X.-L. Qi and S.-C. Zhang, Topological insulators and superconductors, Rev. Mod. Phys. **83**, 1057 (2011).

[2] C.-K. Chiu, J. C. Y. Teo, A. P. Schnyder, and S. Ryu, Classification of topological quantum matter with symmetries, Rev. Mod. Phys. **88**, 035005 (2016).

[3] N. P. Armitage, E. J. Mele, and A. Vishwanath, Weyl and Dirac semimetals in three-dimensional solids, Rev. Mod. Phys. **90**, 015001 (2018).

[4] W. A. Benalcazar, B. A. Bernevig, and T. L. Hughes, Quantized electric multipole insulators., Science **357**, 61 (2017).

[5] W. A. Benalcazar, B. A. Bernevig, and T. L. Hughes, Electric multipole moments, topological multipole moment pumping, and chiral hinge states in crystalline insulators, Phys. Rev. B **96**, 245115 (2017).

[6] Z. Song, Z. Fang, and C. Fang, $(d-2)$-Dimensional Edge States of Rotation Symmetry Protected Topological States, Phys. Rev. Lett. **119**, 246402 (2017).

[7] J. Langbehn, Y. Peng, L. Trifunovic, F. von Oppen, and P. W. Brouwer, Reflection-Symmetric Second-Order Topological Insulators and Superconductors, Phys. Rev. Lett. **119**, 246401 (2017).

[8] F. Schindler, A. M. Cook, M. G. Vergniory, Z. Wang, S. S. P. Parkin, B. A. Bernevig, and T. Neupert, Higher-order topological insulators, Sci. Adv. **4**, eaat0346 (2018).

[9] F. Schindler, Z. Wang, M. G. Vergniory, A. M. Cook, A. Murani, S. Sengupta, A. Y. Kasumov, R. Deblock, S. Jeon, I. Drozdov, H. Bouchiat, S. Guéron, A. Yazdani, B. A. Bernevig, and T. Neupert, Higher-order topology in bismuth, Nat. Phys. **14**, 918 (2018).

[10] C. W. Peterson, W. A. Benalcazar, T. L. Hughes, and G. Bahl, A quantized microwave quadrupole insulator with topologically protected corner states, Nature **555**, 346 (2018).

[11] S. Imhof, C. Berger, F. Bayer, J. Brehm, L. W. Molenkamp, T. Kiessling, F. Schindler, C. H. Lee, M. Greiter, T. Neupert, and R. Thomale, Topolectrical-circuit realization of topological corner modes, Nat. Phys. **14**, 925 (2018).

[12] J. Noh, W. A. Benalcazar, S. Huang, M. J. Collins, K. P. Chen, T. L. Hughes, and M. C. Rechtsman, Topological protection of photonic mid-gap defect modes, Nat. Photon. **12**, 408 (2018).

[13] S. A. A. Ghorashi, T. L. Hughes, and E. Rossi, Vortex and Surface Phase Transitions in Superconducting Higher-order Topological Insulators, Phys. Rev. Lett. **125**, 037001 (2020).

[14] S. A. A. Ghorashi, T. Li, and T. L. Hughes, Higher-Order Weyl Semimetals, Phys. Rev. Lett. **125**, 266804 (2020).

[15] B. Roy, Higher-order topological superconductors in $\mathcal{P}$-, $\mathcal{T}$-odd quadrupolar Dirac materials, Phys. Rev. B **101**, 220506(R) (2020).

[16] B. Roy and V. Juričić, Mixed-parity octupolar pairing and corner majorana modes in three dimensions, Phys. Rev. B **104**, L180503 (2021).

[17] S. A. A. Ghorashi, X. Hu, T. L. Hughes, and E. Rossi, Second-order Dirac superconductors and magnetic field induced Majorana hinge modes, Phys. Rev. B **100**, 020509(R) (2019).

[18] S. H. Kooi, G. van Miert, and C. Ortix, The hybrid-order topology of weak topological insulators, Phys. Rev. B **102**, 041122 (2020).

[19] Y. Wang, M. Lin, and T. L. Hughes, Weak-pairing higher order topological superconductors, Phys. Rev. B **98**, 165144 (2018).

[20] Y. S. Hor, A. J. Williams, J. G. Checkelsky, P. Roushan, J. Seo, Q. Xu, H. W. Zandbergen, A. Yazdani, N. P. Ong, and R. J. Cava, Superconductivity in $Cu_xBi_2Se_3$ and its Implications for Pairing in the Undoped Topological Insulator, Phys. Rev. Lett. **104**, 057001 (2010).

[21] L. Fu and E. Berg, Odd-Parity Topological Superconductors: Theory and Application to $Cu_xBi_2Se_3$, Phys. Rev. Lett. **105**, 097001 (2010).

[22] M. Kriener, K. Segawa, Z. Ren, S. Sasaki, and Y. Ando, Bulk Superconducting Phase with a Full Energy Gap in the Doped Topological Insulator $Cu_xBi_2Se_3$, Phys. Rev. Lett. **106**, 127004 (2011).

[23] S. Sasaki, M. Kriener, K. Segawa, K. Yada, Y. Tanaka, M. Sato, and Y. Ando, Topological Superconductivity in $Cu_xBi_2Se_3$, Phys. Rev. Lett. **107**, 217001 (2011).

[24] A. Yamakage, K. Yada, M. Sato, and Y. Tanaka, Theory of tunneling conductance and surface-state transition in superconducting topological insulators, Phys. Rev. B **85**, 180509(R) (2012).

[25] M. Sato and Y. Ando, Topological superconductors: A review, Rep. Prog. Phys. **80**, 076501 (2017).

[26] L. Fu, Hexagonal Warping Effects in the Surface States of the Topological Insulator Bi_2Te_3, Phys. Rev. Lett. **103**, 266801 (2009).

[27] A. P. Schnyder, S. Ryu, A. Furusaki, and A. W. W. Ludwig, Classification of topological insulators and superconductors in three spatial dimensions, Phys. Rev. B **78**, 195125 (2008).

[28] G. E. Volovik, Topological invariant for superfluid ^{3}He-B and quantum phase transitions, JETP Lett. **90**, 587 (2009).

[29] See Supplemental Material at http://link.aps.org/supplemental/10.1103/PhysRevB.108.094504 for (i) effect of hexagonal warping, (ii) table of allowed perturbations and (iii) plots for superconducting weak TI.

[30] Since our model has C_4^z symmetry, one can also obtain the winding number mod 4 using symmetry indicators. For example, the occupied bands when $M = -2.5 (M = -1.5)$ have one (three) pair(s) of negative inversion eigenvalues having C_4^z eigenvalues of $e^{\pm i\pi/4}$ at the four C_4^z-symmetric momenta. Using the results of [34], these results are consistent with our integral calculations.

[31] We note that this low-energy model has an effective time-reversal symmetry such that $\mathcal{T}^2 = +1$, while the original Hamiltonian has $\mathcal{T}^2 = -1$. When $\mu \neq 1$ the states at $k_z = 0$ combine with other bulk and surface states to restore the full $\mathcal{T}^2 = -1$ symmetry.

[32] L. A. Wray, S.-Y. Xu, Y. Xia, Y. S. Hor, D. Qian, A. V. Fedorov, H. Lin, A. Bansil, R. J. Cava, and M. Z. Hasan, Observation of topological order in a superconducting doped topological insulator, Nat. Phys. **6**, 855 (2010).

[33] L. Aggarwal, P. Zhu, T. L. Hughes, and V. Madhavan, Evidence for higher order topology in Bi and $Bi_{0.92}Sb_{0.08}$, Nat. Commun. **12**, 4420 (2021).

[34] S. Ono, H. C. Po, and H. Watanabe, Refined symmetry indicators for topological superconductors in all space groups, Sci. Adv. **6**, eaaz8367 (2020).

[35] S. Ono, Y. Yanase, and H. Watanabe, Symmetry indicators for topological superconductors, Phys. Rev. Res. **1**, 013012 (2019).

[36] A. Skurativska, T. Neupert, and M. H. Fischer, Atomic limit and inversion-symmetry indicators for topological superconductors, Phys. Rev. Res. **2**, 013064 (2020).

[37] S.-J. Huang and Y.-T. Hsu, Faithful derivation of symmetry indicators: A case study for topological superconductors with time-reversal and inversion symmetries, Phys. Rev. Res. **3**, 013243 (2021).

Supplementary Material: Higher-Order Nodal Hinge States in Doped Superconducting Topological Insulator

Sayed Ali Akbar Ghorashi[1],* Jennifer Cano[1,2], Enrico Rossi[3], and Taylor L. Hughes[4]
[1]*Department of Physics and Astronomy, Stony Brook University, Stony Brook, New York 11794, USA*
[2]*Center for Computational Quantum Physics, Flatiron Institute, New York, New York 10010, USA*
[3] *Department of Physics, William & Mary, Williamsburg, Virginia 23187, USA and*
[4]*Department of Physics and Institute for Condensed Matter Theory, University of Illinois at Urbana-Champaign, IL 61801, USA*

I. HEXAGONAL WARPING

Here, we break the cubic symmetry by the addition of a term of $(\mathcal{O}(\mathbf{k}^3))$ which in the hexagonal lattices represents the effect of hexagonal warping. This will show that the cubic symmetry of the model is not crucial and hinge states can appear in models with reduced symmetries. We use the following higher-order term which breaks in-plane rotation symmetry down to the threefold rotation symmetry,

$$H_{hex} = -\frac{R_1}{2}\big(k_+^3 + k_-^3\big)\kappa_y\sigma_0 \tag{1}$$

We convert it to a lattice representation as follows:

$$H_{hex} = -R_1\big(-4\sin(k_x) - \sin(2k_x) + 6\sin(k_x)\cos(k_y)\big)\kappa_y\sigma_0 \tag{2}$$

The rotational symmetry breaks for any non-zero values of R_1. However, R_1 breaks also both the mirror symmetries along y, z but keeps the M_x intact. As a result we find that hexagonal warping gaps out the $y, z-$hinges but the $x-$hinge remains gapless and only splits the two eight-fold nodes to four four-fold nodes. Fig. 1 shows the x, y, z-hinge states of superconducting phase for weak hexagonal warping R_1.

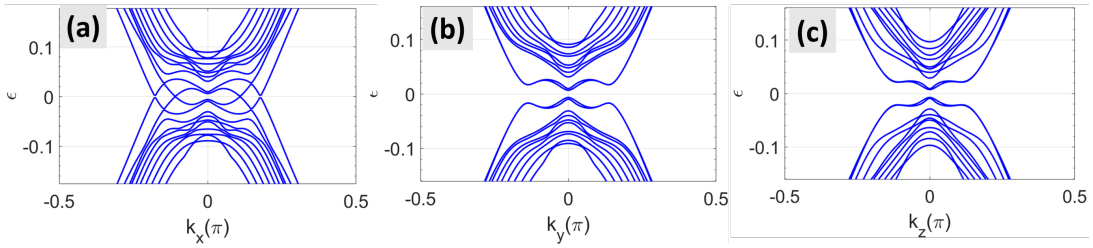

FIG. 1. The hinge spectrum of superconducting TI along the (a) x, (b), y and (c) z directions. We used $M = -1.5$, $\delta_0 = 0.4$, $\mu = 0.8$ and $R_1 = 0.1$.

II. TABLE OF ALL ALLOWED PERTURBATIONS

Here we list table of all trilinear perturbations $\tau^i\kappa^j\sigma^k$ allowed by particle-hole symmetry. This table is produced for the following set of parameters: $M = -1.5$, $\delta_0 = 0.4$, $\mu = 0.8$ (as used in Fig. 3(c1,c2)).

	$M_x = IZX$	$M_y = ZZY$	$M_z = IZZ$	$C_{2x} = ZIX$	$C_{2y} = IIY$	$C_{2z} = ZIZ$	$T = IIY\kappa$	$\mathbb{I} = ZZI$	Surf	Hinge
IIY	0	1	0	0	1	0	0	1	(1,0,1)	(1,1,1)
IXY	1	0	1	0	1	0	0	0	(1,1,1)	(1,1,1)
IYI	0	0	0	1	1	1	0	0	(0,0,0)	(1,1,1)
IYX	0	1	1	1	0	0	1	0	(1,1,1)	(1,1,1)
IYZ	1	1	0	0	0	1	1	0	(1,1,1)	(1,1,1)
IZY	0	1	0	0	1	0	0	1	(1,0,1)	(0,1,0)
XIY(mass)	0	0	0	1	1	1	0	0	(0,0,0)	(0,0,0)
XXY	1	1	1	1	1	1	0	1	(1,1,1)	(1,1,1)
XYI	0	1	0	0	1	0	0	1	(1,0,1)	(1,1,1)
XYX	0	0	1	0	0	1	1	1	(1,1,1)	(0,0,1)
XYZ	1	0	0	1	0	0	1	1	(1,1,1)	(1,0,0)
XZY	0	0	0	1	1	1	0	0	(0,0,0)	(1,1,1)
YIY	0	0	0	1	1	1	1	0	(1,1,1)	(1,1,1)
YXY	1	1	1	1	1	1	1	1	(1,1,1)	(1,1,1)
YYI	0	1	0	0	1	0	1	1	(1,1,1)	(0,1,0)
YYX	0	0	1	0	0	1	0	1	(1,1,0)	(1,1,1)
YYZ	1	0	0	1	0	0	0	1	(0,1,1)	(1,1,1)
YZY	0	0	0	1	1	1	1	0	(1,1,1)	(1,1,1)
ZII	1	1	1	1	1	1	1	1	(1,1,1)	(1,1,1)
ZIX	1	0	0	1	0	0	0	1	(0,1,1)	(1,1,1)
ZIZ	0	0	1	0	0	1	0	1	(1,1,0)	(1,1,1)
ZXI	0	0	0	1	1	1	1	0	(1,1,1)	(0,0,0)
ZXX	0	1	1	1	0	0	0	0	(1,1,1)	(1,1,1)
ZXZ	1	1	0	0	0	1	0	0	(1,1,1)	(1,1,1)
ZYY	1	0	1	0	1	0	1	0	(1,1,1)	(1,1,1)
ZZI	1	1	1	1	1	1	1	1	(1,1,1)	(1,1,1)
ZZX	1	0	0	1	0	0	0	1	(0,1,1)	(1,0,0)
ZZZ	0	0	1	0	0	1	0	1	(1,1,0)	(0,0,1)

TABLE I. "0" and "1" denote the absence or existence of the indicated symmetry. For surface and hinge, it is shown as (x,y,z) vector of the corresponding cuts with "0" and "1" showing gapped and gapless boundaries respectively. For example (1,0,1) for surface means surfaces perpendicular to the x, z remain gapless but the z-surface is gapped. For the hinge (1,0,1) means the hinges parallel to x, z and y are gapless and gapped respectively. The (mass) indicates the perturbation which gaps out all the surface and hinge states.

III. SUPERCONDUCTING WEAK TI

Here we show the corresponding plots of Fig. 3 of the main text for the case of weak topological insulators. This clearly shows that despite the fact that the normal phases of weak and strong TIs possess very different topology, the Majorana hinge modes can universally appear for both the superconducting weak and strong TIs. In fact there is no difference between the superconducting phases of weak ad strong TIs in terms of $1st$-order boundary and topology. Similar to the superconducting strong TI, the first-order topology evolves from trivial to the $W = 3$ and then $W = 2$ topological phases. However, in the $W = 2$ phase, the two Majorana surface cones in the superconducting WTI are positioned at the center and four corners (inset in 2(f1)) while for the superconducting STI they are located at the four sides of the BZ (inset in Fig. 3(f1) of the main text).

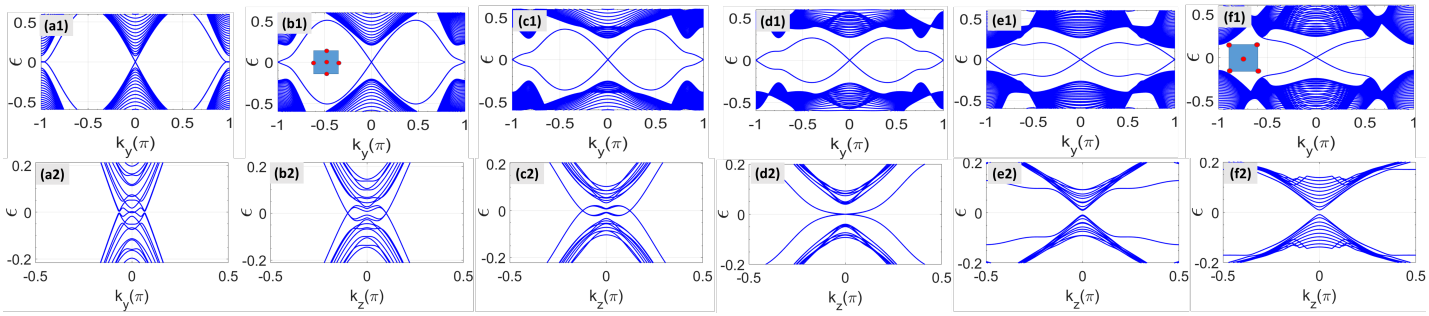

FIG. 2. The evolution of surface (a1-f1) and hinges (a2-f2) states in Superconducting weak TI versus chemical doping μ. $\mu = 0.4, 0.6, 0.8, 1, 1.3, 1.6$, is used for (a-f), respectively. The inset in (b1) and (f1) shows the 2d arrangement of surface nodes. $M = -1.5$, $\delta_0 = 0.4$.

* sayedaliakbar.ghorashi@stonybrook.edu